TISSUE ENGINEERING: Part A
Volume 22, Numbers 3 and 4, 2016
Mary Ann Liebert, Inc.
DOI: 10.1089/ten.tea.2015.0316

termis
Tissue Engineering
& Regenerative Medicine
International Society

ORIGINAL ARTICLE

Angiogenic and Immunomodulatory Properties of Endothelial and Mesenchymal Stem Cells

Sushma Bartaula-Brevik, BDS,[1] Torbjorn O. Pedersen, DDS, PhD,[1] Anna Finne-Wistrand, PhD,[2] Anne Isine Bolstad, DDS, PhD,[1] and Kamal Mustafa, DDS, PhD[1]

It has been suggested that the effect of implanted cells on the local environment is important when selecting the appropriate cell type for tissue regeneration. Our aim was to compare the local tissue response to implanted human mesenchymal stem cells (MSC) and human umbilical vein endothelial cells (EC). MSC and EC were cultured in poly(L-lactide-co-1,5-dioxepan-2-one) scaffolds for 1 week in a bioreactor system, after which they were implanted subcutaneously in NOD/SCID mice. After 3 weeks, scaffolds were retrieved, and the mRNA expression of selected genes involved in hypoxia and inflammation was examined by real-time reverse transcription polymerase chain reaction and correlated with immunofluorescent staining for corresponding proteins. The Toll-like receptor signaling pathway was examined by superarray hybridization. The expression of 53 angiogenesis-related proteins was investigated by a proteome profiler angiogenesis antibody array kit. Vascularization was quantified using immunohistochemistry for CD31. The expression of hypoxia-inducible factors and biomarkers for angiogenesis was more strongly upregulated in response to implanted EC than to MSC, suggesting a higher sensitivity to low oxygen tension among EC. Hypoxic signaling was increased after implantation of EC compared with MSC, leading to a prolonged acute inflammatory phase that promoted ingrowth of vascular cells and establishment of the circulation. Inflammatory cytokines were also differently expressed at the gene and protein levels in the two experimental groups, resulting in altered recruitment of acute and chronic inflammatory cells. The end result of these differences was increased vessel formation within the constructs in the EC group.

Introduction

For vascular tissue engineering, as well as in regeneration of parenchymal tissue, such as muscle or bone, extensive efforts have been made to learn how to generate functional vascular supply for implanted cells. These efforts have been made based on the premise that implanted cells cannot survive, differentiate, and regenerate lost tissue without an immediate functional blood supply. In situations where the circulation has been compromised, cell therapy has been explored with the aim of re-establishing circulation to regenerate the damaged tissue. Hematopoietic stem cells have demonstrated cardiomyogenic potential after implantation in ischemic cardiac tissue,[1] and endothelial progenitor cells have been the subjects of extensive research efforts for their potential in cardiovascular regeneration.[2]

Bone marrow mesenchymal stem cells (MSC) are the most widely applied cells in cell therapy due to their availability and differentiation potential. The interaction between MSC and vascular cells has been extensively explored, and MSC have diverse roles in the vascularization of tissue through either direct contact or indirect signaling. The autocrine and paracrine effects of MSC initiate release of cytokines, growth factors, and extracellular matrix proteins.[3,4] In an attempt to generate functional vessels that can be connected with the local circulation after implantation, coculture systems have been used with vascular cells grown with supporting cells, such as smooth muscle cells (SMC) or MSC.[5–7]

The proliferation and maturation of endothelial cells (EC) and surrounding matrix depend on local oxygen supply[8,9] and the crosstalk between EC and immune cells, which

[1]Department of Clinical Dentistry, University of Bergen, Bergen, Norway.
[2]Department of Fibre and Polymer Technology, KTH Royal Institute of Technology, Stockholm, Sweden.

results in release of cytokines and chemokines.[10] The direct contribution of implanted vascular or MSC to tissue regeneration is not well described in most studies, although both cell types contribute to development and repair of the majority of the body tissues. Several authors have suggested that the favorable effect of implanting cells or bioactive molecules on regeneration in a damaged area is as much the result of creating a favorable microenvironment for cell migration and proliferation as it is of direct deposition of extracellular matrix components by the implanted cells.[11,12]

It is clear, however, that the basis for healthy tissue is a functional circulation, which in turn applies to both parenchymal and vascular tissue engineering. All implanted cells are exposed to a hypoxic environment after implantation due to the acute inflammation following the surgical procedure, as well as the initial absence of blood vessels. The cellular response to hypoxia is therefore a key in facilitating an adequate postoperative inflammatory reaction and the establishment of a functional blood supply. These cellular events are closely connected to each other and crucial for ensuring vital and healthy tissue regeneration.

Based on this, our hypothesis was that MSC and EC respond differently to the hypoxic environment created when cells are implanted *in vivo* and that the inflammatory response as well as the establishment of the blood supply are different between the two cell types. The aims of the study therefore were first to compare the effect of implanting MSC and EC on the expression of inflammatory cytokines and the migration of acute and chronic inflammatory cells and second to compare the effect of implanted cells on expression of vascular factors and development of the circulation.

Materials and Methods

Fabrication of scaffolds

Poly(L-Lactide-*co*-1,5-dioxepan-2-one) [poly (LLA-co-DXO)] was synthesized, and scaffolds were prepared as previously described.[13,14] Briefly, a solvent casting/particulate leaching method was used to produce poly (LLA-co-DXO) porous scaffolds with pore sizes of 90–500 μm, 12 mm diameter, and 1.5 mm thick. The sterilization of scaffolds was carried out in a pulsed electron accelerator operating at 6.5 MeV (Mikrotron, Acceleratorteknik, The Royal Institute of Technology, Stockholm, Sweden), with radiation of 2.5 Mrad dose in an inert atmosphere.

Cell culture

Primary human MSC were purchased from StemCell Technologies. Flow cytometry was done to confirm the purity of the cells, >90% of the cells expressed CD29, CD44, CD105, and CD166 and <1% expressed CD14, CD34, and CD45. The MSC were cultured in MesenCult® complete medium (StemCell Technologies) following the manufacturer's instructions.

Human umbilical vein EC were purchased from Lonza (Clonetics®). They were expanded in endothelial cell growth medium (EGM®) (Lonza) containing 500 mL endothelial cell basal medium and supplements, 10 mL fetal bovine serum, 2 mL bovine brain extract, 0.5 mL human endothelial growth factor, 0.5 mL hydrocortisone, and 0.5 mL GA-1000. The MSC and EC were cultured at 37°C and 5% CO_2 and were used between passages 2 and 5.

In vivo *implantation*

The scaffolds were preseeded with cells before *in vivo* implantation and were treated as previously described.[7,15] Briefly, the scaffolds were divided into two groups: MSC and EC, prewet with respective complete medium and incubated overnight at 37°C and 5% CO_2. In total, 5×10^5 cells were seeded per scaffold in each group. An orbital shaker (Eppendorf®) was used to facilitate homogeneous distribution of cells. The scaffolds loaded with cells were kept in an incubator overnight to allow cell attachment. The following day, scaffolds were transferred to separate modified spinner flasks (Wheaton Science) for 1 week in a dynamic culture system with 50 rpm. After 1-week *in vitro* culture, 6-mm discs were punctured from the center of the scaffold with a dermal skin puncher and then implanted *in vivo*. For evaluating seeding efficiency of MSC and EC, the cells were seeded in scaffold as described above, and after 1 h, the scaffolds were removed from the wells, and unattached cells were counted by an Automated Cell Counter (Invitrogen). Cell seeding efficiency was calculated by the following equation[16]:

$$\text{Cell seeding efficiency}\% = \left(1 - \frac{\text{number of unattached cells}}{\text{number of seeded cells}}\right)\times 100$$

The animal experiments were approved by the Norwegian Animal Research Authority and conducted according to the European Convention for the Protection of Vertebrates used for Scientific Purposes (local approval no. 3029). Nonobese diabetic/severe combined immunodeficient (NOD/SCID) mice ($n=15$) were purchased from Taconic Farms (Bomholtgård Breeding and Research Center). The animals were kept in polystyrene cages containing wood shavings in a climate-controlled environment with 12-h dark–12-h light cycles and fed with standard rodent chow and water *ad libitum*. Animals were 6–8 weeks old at the time of surgery. The animals were anesthetized with an intramuscular injection of 20 μL of Rompun (xylazine) (20 mg/mL) (Bayer Healthcare) and Narketan (ketamine) (Vétoquinol) in 1:2 ratio. On the back of the mice, a 2.5-cm incision was made, providing sufficient space for subcutaneous implantation of scaffolds. A scaffold for each experimental group (MSC or EC) was placed in the mouse, with a total of six mice used for each time point. Wounds were closed with Vetbond™ Tissue Adhesive (n-butyl cyanoacrylate) (3M™). After 3-week implantation, animals were euthanized with deep isoflurane (Schering Plough) anesthesia, followed by cervical dislocation, after which the implanted scaffolds were carefully dissected and retrieved. The samples were then divided and further processed either for real-time reverse transcription polymerase chain reaction (RT–PCR) analysis and western blotting or for histological embedding.

Real-time RT–PCR

E.Z.N.A.® Total RNA Kit (Omega Bio-Tek) was used to isolate the RNA from the samples. Quantifications and determination of RNA purity were performed with a NanoDrop Spectrophotometer (Thermo Scientific NanoDrop Technologies). A high-capacity cDNA Archive Kit (Applied Biosystems) was used for the reverse transcription reaction. Total RNA (1000 ng) was mixed with nuclease-free water,

reverse transcriptase buffer, random primers, dNTP, and MultiScribe reverse transcriptase. Standard enzyme and cycling conditions were applied for 2 min at 50°C and 20 s at 95°C, followed by 1 s at 95°C and 20 s at 60°C per cycle (40 cycles). cDNA corresponding to 10 ng mRNA in each reaction was prepared in duplicate since the standard deviation between the duplicates was minimal for each target gene. Real-time RT–PCR was performed on a StepOnePlus™ Real-Time PCR System (Applied Biosystems). Mouse-specific TaqMan® gene expression assays (Applied Biosystems) were used to evaluate postimplanted constructs. The preimplanted constructs were also assessed to evaluate baseline expression of inflammatory and hypoxic markers. For this, human-specific TaqMan gene expression assays (Applied Biosystems) were used. Data analysis was performed with a comparative Ct method, with GAPDH as endogenous control.[17]

Superarray analysis was performed for the mouse Toll-like receptor (TLR) pathway Rt^2 Profiler PCR Arrays (SuperArray Bioscience). Rt^2 PCR Array First Strand Kit (SuperArray Bioscience) was used for cDNA synthesis. PCR was done on a StepOnePlus Real-Time PCR System (Applied Biosystems) with Rt^2 Real-Time SyBR Green/Rox PCR Mix (SuperArray Bioscience).

Immunofluorescent staining

The remaining half of the sample was immediately embedded in optimal cutting temperature compound (Tissue-Tek® O.C.T.; Sakura Finetek) and kept at −80°C. Eight-micrometer-thick cryosectioning was done with Leica CM3050 S (Leica Microsystems) at −24°C. Sections were obtained from the middle part of the scaffolds and were used for immunostaining. Sections from 3-week samples were incubated with primary antibodies in blocking buffer overnight at 4°C and with secondary antibodies for 2 h the following day. The nuclei were counterstained with DAPI (1:1000) for 2 min, and the slides were mounted with ProLong® Gold Antifade Reagent (Invitrogen) before imaging. Rabbit polyclonal anti-mouse interleukin (IL)-1β (Abcam), rat monoclonal anti-mouse neutrophil (NIMP) (Abcam), rabbit polyclonal anti-mouse IL-6 (Abcam), rat monoclonal anti-mouse CD11b (BD Biosciences), and rat monoclonal anti-mouse CD31 (BD Biosciences) were used as primary antibodies. Goat anti-rabbit FITC (Santa Cruz Biotechnology) and Alexa Fluor 546 goat anti-rat (Invitrogen) were used as secondary antibodies. Double staining with IL-1β and NIMP was performed to identify the number of IL-1β-positive cells and the number of neutrophils, respectively. Double staining with IL-6 and CD11b was performed to colocalize macrophages or monocyte-derived cells and their production of IL-6. CD31 staining was performed to allow determination of the total area fraction of vessels.

Quantification of immunostaining

Five sections from one scaffold were mounted on each slide. Each section on the slides was divided into five measuring grids starting from top to bottom in the vertical direction. Five sections on each slide (average for the mouse) and five measuring grids in each section (average for the section) were used for image quantification. Images were taken with a Zeiss AxioVision 4.8.1 at 10× magnification, and the files were exported as JPEG standard. The measuring grids in each section were noted carefully to avoid any overlap while taking the images. In each section, the areas with no cells were excluded. NIS Elements AR 3.2 software was used for quantifications. First, the threshold was defined for each channel: red, green, and blue. Next, to avoid misinterpretation, all the channels were simultaneously referred before counting the cells. The blue channel was referred continuously to visualize the nuclei, and then, the counting was done in the red and green channels separately. Finally, colocalized cells were counted for red and green fluorescent staining together. The number of counted cells was exported to a Microsoft Excel (Microsoft Corporation) file before statistical analysis was performed. For quantification of CD31 immunostaining, images were taken at 20× magnification, and the total area fraction of vessel was quantified.

Western blotting

Protein extraction was performed following the protocol of Chomczynski.[18] Briefly, isopropanol was added to the organic phase (extracted during RNA isolation) for protein precipitation. Precipitate was washed with ethanol and dissolved in 0.5% sodium dodecyl sulfate (SDS) solution. NanoDrop Spectrophotometer (Thermo Scientific NanoDrop Technologies) was used to quantify and determine protein purity. A total of 30 μg protein was mixed with 4× Laemmli sample buffer (Bio-Rad Laboratories) and loaded on 4–15% Mini-PROTEAN® TGX™ Precast Gel (Bio-Rad) for electrophoresis. Transfer was done with PVDF transfer membranes (TRANS-Blot® Turbo™ System; Bio-Rad). The membranes were blocked overnight at 4°C and incubated the next day with primary antibodies (Santa Cruz): anti-mouse hypoxia-inducible factor 1-alpha (HIF-1α), anti-mouse aryl hydrocarbon receptor nuclear translocator (ARNT), and anti-mouse GAPDH in blocking buffer overnight at 4°C and the following day with secondary antibody: horseradish peroxidase-conjugated goat anti-rabbit IgG (Bio-Rad) for 1 h. Immunoblotting bands were visualized by Immun-Star™ WesternC™ Chemiluminescence Kits, and a Gel Doc™ EZ System (Bio-Rad) was used for imaging and protein-band assay.

Proteome profiling

The Mouse Angiogenesis Array (R&D Systems, Inc.) was used to detect the expression of 53 angiogenesis-related proteins in the experimental groups. These Proteome Profiler Arrays were handled according to the manufacturer's protocol. Briefly, the protein extraction was done, and 100 μg of total protein was mixed with a cocktail of biotinylated detection antibodies and then incubated with a nitrocellulose membrane spotted with capture antibodies in duplicate. Protein detection antibodies bound to the capture antibody were detected using streptavidin–HRP and chemiluminescent detection reagents. The Gel Doc EZ System (Bio-Rad) was used for imaging. The mean spot pixel density was quantified using image software analysis.

Statistical analyses

SPSS Statistics 21 (IBM) was applied for statistical processing and analysis. Two groups, MSC and EC, were compared with the independent samples *t*-test. The significance level was set to $p < 0.05$ for all statistical analyses, with $n = 6$ for each group.

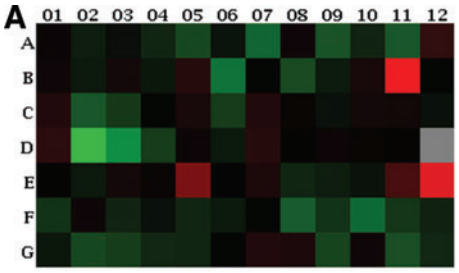

B

Layout	01	02	03	04	05	06	07	08	09	10	11	12
A	Agfg1 1.05	Btk -1.23	Casp8 -1.04	Ccl2 -1.19	Cd14 -1.40	Cd80 -1.07	Cd86 -1.60 *	Cebpb 1.06	Chuk -1.5	Clec4e 1.17	Csf2 -1.48	Csf3 1.28
B	Cxcl10 1.07	Eif2ak2 -1.11	Elk1 1.10	Fadd 1.10	Fos 1.2	Hmgb1 -1.70 **	Hras1 -1.01	Hspa1a -1.41	Hspd1 -1.11	Ifnb1 1.12	Ifng 3.26	Ikbkb -1.01
C	Il10 1.19	Il12a -1.49	Il1a -1.30	Il1b -1.01	Il1r1 1.12	Il2 -1.32	Il6 1.19	Il6ra 1.03	Irak1 -1.05	Irak2 1.09	Irf1 1.08	Irf3 -1.06
D	Jun 1.25 *	Lta -2.56	Ly86 -1.93 *	Ly96 -1.33 *	Map2k3 1.06	Map2k4 -1.11	Map3k1 1.21	Map3k7 1.01	Mapk8 1.06	Mapk8ip 3 1.03	Mapk9 1.01	Muc13 -1.13
E	Myd88 1.02	Nfkb1 -1.11	Nfkb2 1.10	Nfkbia 1.04	Nfkbib 1.78	Nfkbil1 1.00	Nfrkb 1.15	Nr2c2 -1.18	Peli1 -1.13	Pglyrp1 -1.07	Ppara 1.42	Ptgs2 2.81
F	Rel -1.28 *	Rela 1.06	Ripk2 -1.17	Tbk1 -1.07	Ticam1 -1.18	Ticam2 -1.11	Tirap -1.01	Tlr1 -1.52 *	Tlr2 -1.27 *	Tlr3 -1.63 *	Tlr4 -1.28 *	Tlr5 -1.16
G	Tlr6 -1.09	Tlr7 -1.40	Tlr8 -1.34 *	Tlr9 -1.19	Tnf -1.18	Tnfaip3 -1.01	Tnfrsf1a 1.18	Tollip 1.14	Tradd -1.37 *	Traf6 1.07	Ube2n -1.41 *	Ube2v1 -1.19

FIG. 1. Alteration in the Toll-like receptor (TLR) signaling pathway. **(A)** Rt^2 Profiler TLR signaling polymerase chain reaction (PCR) array following 3 weeks of implantation *in vivo*. Heat maps representing the relative expression levels of all genes involved in the mouse TLR signaling pathway. Increased and decreased fold changes in endothelial cell (EC) constructs compared with mesenchymal stem cell (MSC) constructs are represented by *red* and *green squares*, respectively. **(B)** Gene layout of heat maps and data are presented as $*p<0.05$, $**p<0.01$. Color images available online at www.liebertpub.com/tea

Results

Alteration in the TLR pathway

The evaluation of genes related to the mouse TLR pathway showed that 49 genes were downregulated and 35 genes were upregulated, with a fold change more than one in the EC group compared with the MSC group (Fig. 1A, B).

Release of inflammatory cytokines

Inflammation was evaluated through the release of pro- and anti-inflammatory cytokines. RT–PCR (human-specific genes) of preimplanted constructs showed higher mRNA expression of the genes encoding *IL-1β* and *IL-10* in the MSC group, whereas the expression of the gene *IL-6* was similar in both groups (not shown). RT–PCR for mouse-specific genes was performed after 3 weeks of implantation. Decreased mRNA expression of the genes enconding the proinflammatory cytokines, *IL-1β* and *IL-6*, was observed in EC constructs ($p<0.05$) (Fig. 2B, C). However, the mRNA expression of the gene encoding the anti-inflammatory cytokine *IL-10* was upregulated in EC constructs compared with MSC constructs ($p<0.01$) (Fig. 2D).

Inflammatory cell recruitment

The acute and chronic inflammatory cell recruitment was evaluated by immunofluorescence staining and systematic

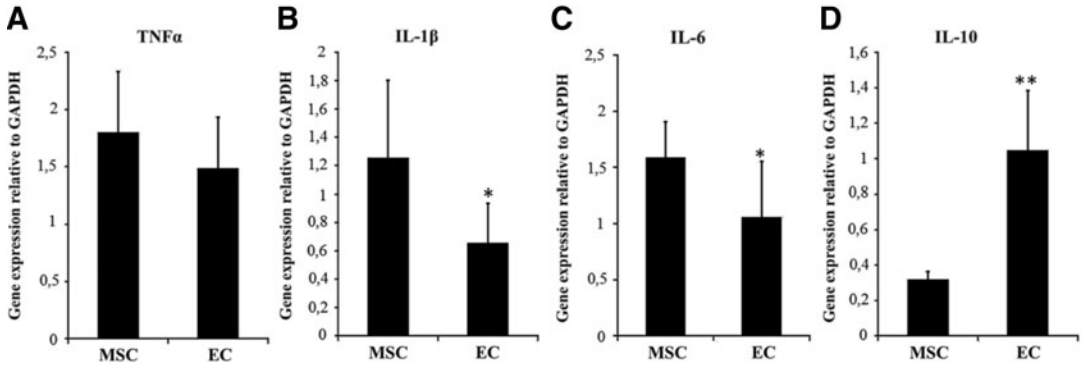

FIG. 2. Real-time reverse transcription (RT)–PCR for mouse-specific genes after 3 weeks of implantation *in vivo*. Relative gene expression of the genes encoding the inflammatory cytokines **(A)** tumor necrosis factor-alpha (TNFα), **(B)** interleukin-1-beta (*IL-1β*), **(C)** *IL-6*, and **(D)** IL-10 comparing MSC and EC constructs. Data presented as mean ± standard deviation ($n=6$). $*p<0.05$, $**p<0.01$.

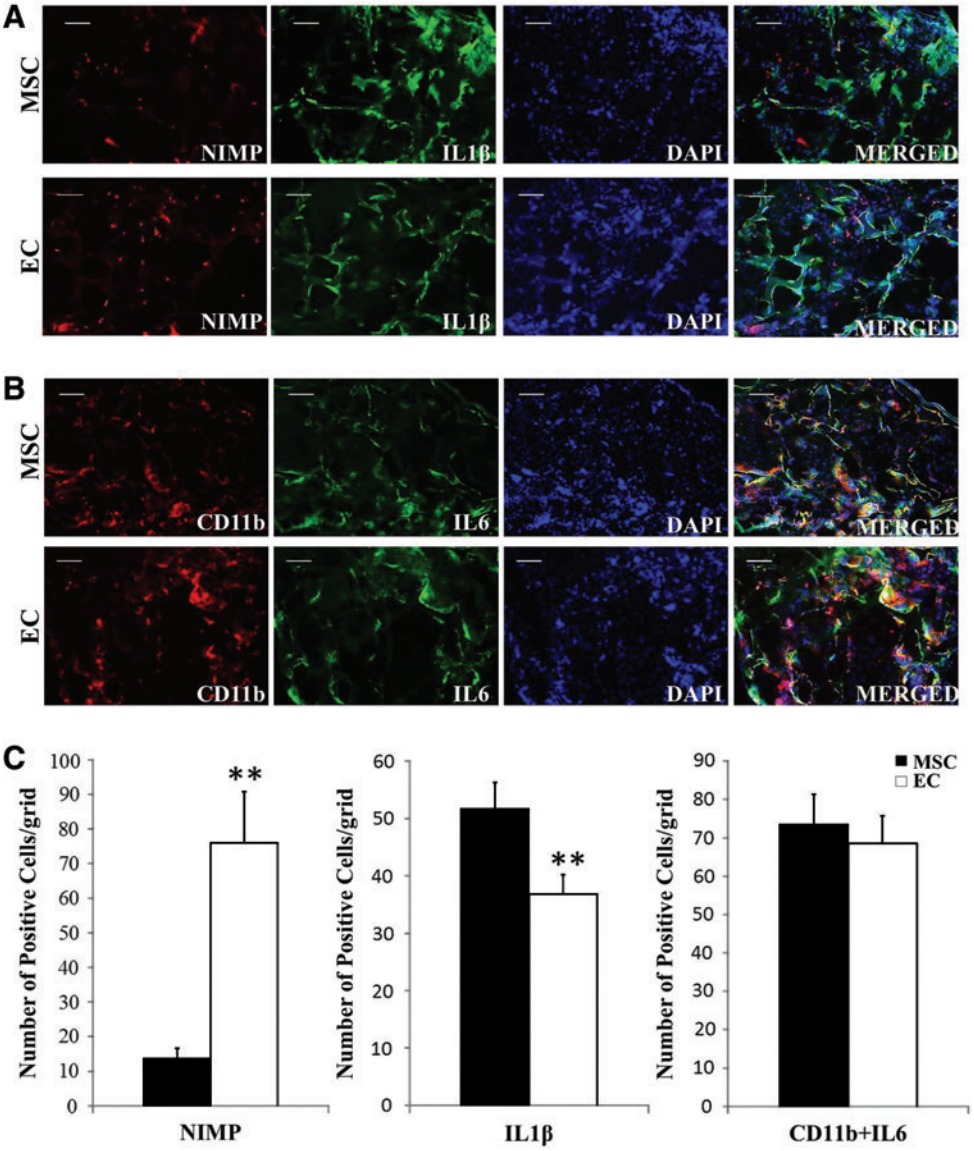

FIG. 3. Inflammatory cell recruitment to tissue-engineered constructs after 3 weeks of implantation *in vivo*. **(A)** Neutrophil transmigration to the constructs and expression of IL-1β. Representative fluorescent images of monoclonal antineutrophil antibody (NIMP) and IL-1β staining from MSC and EC constructs using mouse-specific antibodies. **(B)** Colocalization of monocyte-derived cells and IL-6. Representative fluorescent images of mouse-specific antibodies CD11b and IL-6 double staining for multinucleated cells (10× magnification, scale bar = 100 μm). **(C)** Five sections from each mouse and five images for each section were used for image quantification. The number of neutrophils was significantly higher in the EC group (**$p < 0.01$, $n = 6$). The number of IL-1β-positive cells was lower in the EC group (**$p < 0.01$, $n = 6$). The number of CD11b- and IL-6-positive cells was decreased in the EC group, but this was not statistically significant. Color images available online at www.liebertpub.com/tea

quantification. Cells stained positive with antineutrophil antibody were found scattered all over the constructs, predominantly in the EC group (Fig. 3A) ($p < 0.01$). Fewer IL-1β-positive cells were seen in the EC group than in the MSC group ($p < 0.01$) (Fig. 3C). Double staining for monocyte-derived cells (CD11b) and IL-6 showed fewer positive cells in the EC group, but this difference was not statistically significant (Fig. 3C). Cells stained positive with CD11b and IL-6 were found in close proximity to the scaffold and may have aided in the degradation process (Fig. 3B).

Cellular response to a hypoxic environment

To evaluate the response to hypoxia after implantation, the mRNA expression of the genes encoding HIF-1α and ARNT was analyzed. Both markers were significantly upregulated in EC constructs after 3 weeks of implantation (Fig. 4A, B). On the contrary, western blotting showed lower protein level of HIF-1α in EC constructs, while the protein level of ARNT was higher in EC constructs compared with MSC constructs (Fig. 4E). The mRNA expression of the gene encoding mTOR was significantly upregulated in the EC group (Fig. 4D). The mRNA expression of the genes encoding human HIF-1α and ARNT was significantly higher in the EC group before implantation compared to the MSC group.

Angiogenic properties of MSC and EC

To evaluate the angiogenic properties of the cells after 3 weeks of implantation, proteome profiling was done (Fig. 5A). The histogram generated after the mean spot pixel density quantification revealed that of the 53 related proteins for angiogenesis, 10 proteins were highly regulated. The proteins related to vascular development were higher in the EC group compared with the MSC group (Fig. 5B). In addition, the total area fraction of vessel formation was quantified to determine the influence of implanted cells on establishment of the vasculature. The EC constructs had a higher density of blood vessel formation, as evaluated by CD31 immunostaining, and the total vessel area fraction was significantly higher ($p < 0.01$) (Fig. 5C).

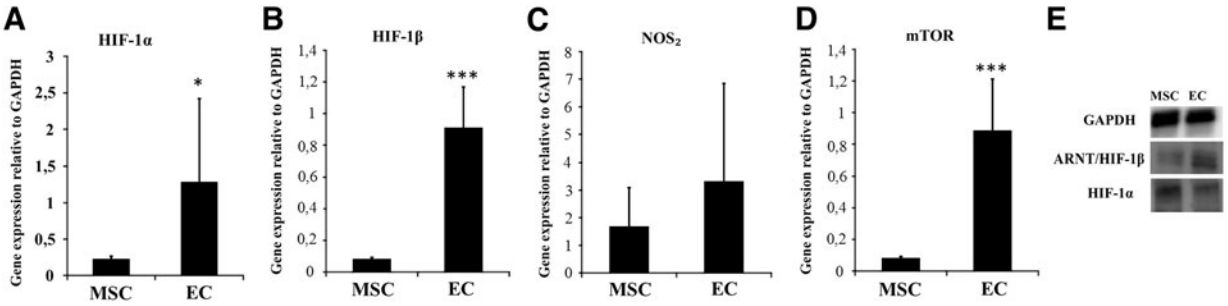

FIG. 4. Relative gene and protein expression of hypoxic markers after 3 weeks of implantation *in vivo*. Real-time RT–PCR for mouse-specific genes **(A)** hypoxia-inducible factor 1-alpha (*HIF-1α*), **(B)** HIF-1β/aryl hydrocarbon receptor nuclear translocator (*ARNT*), **(C)** nitric oxide synthase 2 (*NOS_2*), and **(D)** mammalian target of rapamycin (*mTOR*). **(E)** Relative protein expression of HIF-1α and HIF-1β in MSC and EC constructs.

Discussion

In cell therapy, the release of inflammatory cytokines facilitates vascularization and recruitment of leukocytes in the first phase after implantation. If the balance between pro- and anti-inflammatory cytokines is favorable, this leads to tissue organization and regeneration.[19,20] The aims of this study were to evaluate and compare the initiation of angiogenesis and early inflammation after implantation of cell/scaffold constructs using two different cell types. The cells were grown under the same culture conditions before implantation. The seeding efficiency of the two cell types in the scaffold was similar. After implantation of the cells, host tissue response was evaluated. The NOD/SCID mouse model was chosen as it allows human cells to grow and differentiate, and previous studies have shown that these

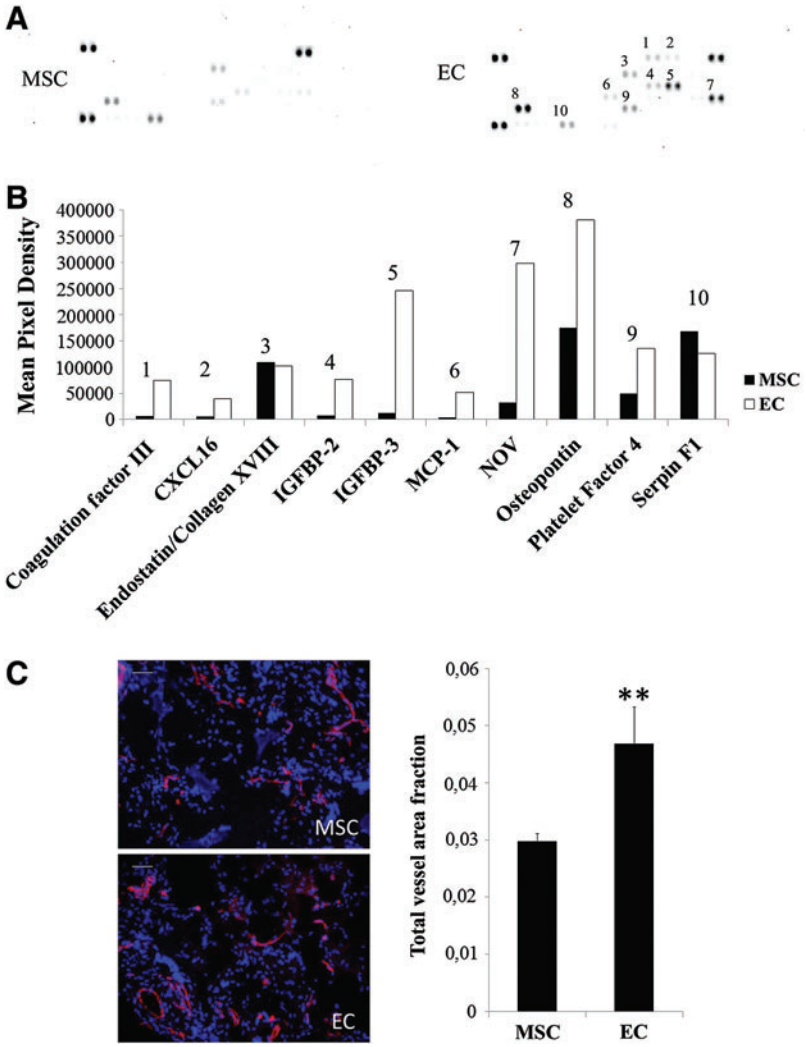

FIG. 5. Angiogenic properties of MSC and EC were evaluated after 3 weeks of implantation *in vivo*. **(A)** The proteome profiler mouse angiogenesis kit was used to access the relative levels of 53 angiogenesis-related proteins in MSC and EC constructs; highly regulated proteins were marked from 1 to 10. **(B)** Histogram profile of selected proteins generated by quantifying the mean spot pixel density from the arrays using image software analysis. **(C)** CD31 immunostaining of blood vessels (*red*) at 20× magnification (scale bar = 50 μm) and total area fraction of $CD31^+$ cells after 3 weeks of implantation. The area fraction of vessel formation was significantly higher in the EC group (**$p < 0.01$). Nuclei were stained with DAPI (*blue*). Color images available online at www.liebertpub.com/tea

animals can produce monocyte-derived cells and neutrophils.[21] This moderately immunocompromised murine model thus also allows investigation of the early innate immune response to implantation. Response of the implanted MSC and EC to hypoxia was investigated, as was their effect on the local microenvironment, subsequent recruitment of acute and chronic inflammatory cells, and establishment of blood vessels in the area of the implant. The mouse-specific markers were used to evaluate the host response toward the implanted cells.

MSC have been reported to express TLR that may play a role in immune regulation. TLR priming of MSC results in two active phenotypes, MSC1 and MSC2. TLR4-primed MSC (MSC1) expresses proinflammatory cytokines, whereas TLR3-primed MSC (MSC2) regulates anti-inflammatory cytokines.[22] TLR activation in MSC could produce inflammatory mediators, such as IL-1β, IL-6, IL-8/CXCL8, and CCL5, resulting in recruitment of inflammatory cells.[23] TLR and its ligands may also induce the proliferation and differentiation of MSC.[24] TLR ligand activation on EC regulates the expression of TLR1, TLR3, and TLR4 and downstream production of IL-6.[25] The superarray analysis in the present study for the mouse TLR pathway demonstrated downregulation of the genes encoding TLR1, TLR2, TLR3, TLR4, and TLR8 in the EC group compared with the MSC group ($p < 0.05$). The downstream production of TLR was evaluated by looking at mRNA expression of the genes encoding IL-1β, IL-6, and IL-10. Macrophages are subdivided into M1 and M2, according to their ability to produce different cytokines. M1 releases proinflammatory cytokines in contrast to M2, which releases anti-inflammatory cytokines.[26] The mRNA expression of genes encoding proinflammatory markers, such as IL-1β and IL-6, was significantly downregulated in the EC group compared with the MSC group ($p < 0.05$), and EC contributed to the anti-inflammatory effects via upregulated mRNA expression of the *IL-10* gene ($p < 0.01$). These findings suggest that EC can switch the cytokine expression of macrophages to the anti-inflammatory M2 phenotype.

Copolymer scaffolds provide temporary support in tissue engineering constructs as they degrade over time. A foreign-body giant cell reaction mediates degradation of the scaffold along with buildup of new extracellular matrix protein and recruitment of granulocytes, MSC, and monocyte-derived cells.[27] Sung *et al.* found no significant difference in inflammatory cell recruitment by different copolymers after 2–4 weeks of implantation *in vivo*. Furthermore, they showed that inflammatory cell recruitment had a positive correlation with angiogenesis.[28] Similarly, we demonstrated the recruitment of inflammatory cells adjacent to the scaffold after 3 weeks' implantation. Neutrophils are the first line of defense in acute inflammation. After 3 weeks' implantation, we observed that neutrophil transmigration to the EC constructs was significantly higher than in MSC constructs ($p < 0.01$). Our previous study also found that coculture of MSC with EC resulted in more leukocyte transmigration to the construct via the TLR pathway.[29] Furthermore, IL-1β-positive monocyte-derived cells were decreased in the EC group relative to the MSC group ($p < 0.01$), while the number of IL-6- and CD11b-positive cells was higher in the MSC group. Multinucleated giant cells were found in proximity to the scaffold, aiding in degradation. Neutrophils[30] and CD11b-positive cells[31] have been shown to increase angiogenesis, and the differing inflammatory cell recruitment seen between the experimental groups may also have contributed to the difference in vascularization.

Tissue ischemia is one cause of failure of tissue-engineered constructs. The inflamed microenvironment is highly metabolic and has higher oxygen consumption, leading to low oxygen tension. Additionally, hypoxia also mediates acute and chronic inflammation. Hypoxia in the surrounding environment activates the release of HIF, a transcription factor for angiogenesis.[32–34] The preimplanted EC group showed upregulation of human hypoxia-related genes. The paracrine effect of these cells could have influenced the host microenvironment to promote angiogenesis. The mRNA expression of the *HIF-1α* and *HIF-1β* genes was significantly upregulated in the EC group, $p < 0.05$ and $p < 0.001$, respectively. The upregulation in HIF genes promotes angiogenesis. In addition, HIF-1α protein levels were higher in the MSC group. The initiation of angiogenesis leads to higher oxygen saturation in the construct area, which could have resulted in lower *HIF-1α* protein expression in EC constructs. However, it has been reported that HIF-1β is less sensitive to change in oxygen tension.[35] In the present study, we found that mRNA expression and the protein level of HIF-1β were upregulated in the EC group compared to the MSC group.

NOS_2/iNOS has also been reported as a hypoxia-inducible gene. It regulates vascular homeostasis and inflammation and may also promote HIF-1α stabilization and activate downstream gene expression.[36,37] We observed upregulation of the *NOS_2* gene in the EC group compared with the MSC group, promoting angiogenesis. The mRNA expression of the gene encoding mTOR was higher in the EC constructs, which also leads to vascularization of the constructs. The mTOR pathway regulates cell proliferation, adhesion, migration, metabolism, and survival, and mTOR modulates angiogenic factors by activating either HIF-1α or NOS_2.[38]

Proteome profiling was performed to compare the angiogenic factors released by EC and MSC constructs after 3 weeks' implantation. Among all differentially regulated proteins, osteopontin, nephroblastoma overexpressed (NOV), and insulin-like growth factor-binding protein-3 (IGFBP-3) highly upregulated in EC constructs. Osteopontin is a potent angiogenic factor, which promotes proliferation, migration, and capillary formation of EC.[39] NOV is highly expressed in SMC of the arterial vessel wall and supports cell adhesion, migration, and survival of EC, resulting in neovascularization.[40] IGFBP-3 has diverse roles in angiogenesis. It regulates proangiogenic molecules and induces capillary formation *in vivo*.[41] In 1999, Dawson *et al.* identified a serine protease inhibitor, SERPIN F1, as an antiangiogenic factor.[42] SERPIN F1 was increased following MSC implantation in the present work. The release of proangiogenic proteins was higher than antiangiogenic factors after implantation of EC, which was reflected in the increased area of vessel formation.

Conclusions

Implantation of EC resulted in downregulation of TLR and biomarkers associated with acute inflammation. Significantly higher numbers of neutrophils were present after 3 weeks' implantation, which was associated with hypoxia-induced signaling. In addition, increased vascular ingrowth

was found after implantation of EC. These findings suggest that implantation of EC stimulates hypoxic signaling pathways, which leads to a prolonged acute inflammatory phase compared with implantation of MSC. This promotes ingrowth of vascular cells and establishment of the circulation.

Acknowledgments

This study was supported by the VascuBone project, European Union FP7; grant no. 242175. The authors thank Dr. Michele Cottler-Fox, University of Arkansas for Medical Sciences, Little Rock, USA, for constructive comments on the article.

Disclosure Statement

No competing financial interests exist.

References

1. Jackson, K.A., Majka, S.M., Wang, H., Pocius, J., Hartley, C.J., Majesky, M.W., Entman, M.L., Michael, L.H., Hirschi, K.K., and Goodell, M.A. Regeneration of ischemic cardiac muscle and vascular endothelium by adult stem cells. J Clin Invest **107,** 1395, 2001.
2. Kawamoto, A., and Losordo, D.W. Endothelial progenitor cells for cardiovascular regeneration. Trends Cardiovasc Med **18,** 33, 2008.
3. Baraniak, P.R., and McDevitt, T.C. Stem cell paracrine actions and tissue regeneration. Regen Med **5,** 121, 2010.
4. Melchiorri, A.J., Nguyen, B.N., and Fisher, J.P. Mesenchymal stem cells: roles and relationships in vascularization. Tissue Eng Part B Rev **20,** 218, 2014.
5. Hegen, A., Blois, A., Tiron, C.E., Hellesoy, M., Micklem, D.R., Nor, J.E., Akslen, L.A., and Lorens, J.B. Efficient in vivo vascularization of tissue-engineering scaffolds. J Tissue Eng Regen Med **5,** e52, 2011.
6. Au, P., Tam, J., Fukumura, D., and Jain, R.K. Bone marrow-derived mesenchymal stem cells facilitate engineering of long-lasting functional vasculature. Blood **111,** 4551, 2008.
7. Pedersen, T.O., Blois, A.L., Xing, Z., Xue, Y., Sun, Y., Finne-Wistrand, A., Akslen, L.A., Lorens, J.B., Leknes, K.N., Fristad, I., and Mustafa, K. Endothelial microvascular networks affect gene-expression profiles and osteogenic potential of tissue-engineered constructs. Stem Cell Res Ther **4,** 52, 2013.
8. Carmeliet, P. Angiogenesis in health and disease. Nat Med **9,** 653, 2003.
9. Jain, R.K. Molecular regulation of vessel maturation. Nat Med **9,** 685, 2003.
10. Kaplanski, G., Fabrigoule, M., Boulay, V., Dinarello, C.A., Bongrand, P., Kaplanski, S., and Farnarier, C. Thrombin induces endothelial type II activation *in vitro*: IL-1 and TNF-alpha-independent IL-8 secretion and E-selectin expression. J Immunol **158,** 5435, 1997.
11. Greco, S.J., and Rameshwar, P. Microenvironmental considerations in the application of human mesenchymal stem cells in regenerative therapies. Biologics **2,** 699, 2008.
12. Barthes, J., Ozcelik, H., Hindie, M., Ndreu-Halili, A., Hasan, A., and Vrana, N.E. Cell microenvironment engineering and monitoring for tissue engineering and regenerative medicine: the recent advances. Biomed Res Int **2014,** 921905, 2014.
13. Odelius, K., Plikk, P., and Albertsson, A.C. Elastomeric hydrolyzable porous scaffolds: copolymers of aliphatic polyesters and a polyether-ester. Biomacromolecules **6,** 2718, 2005.
14. Dånmark, S., Finne-Wistrand, A., Wendel, M., Arvidson, K., Albertsson, A.-C., and Mustafa, K. Osteogenic differentiation by rat bone marrow stromal cells on customized biodegradable polymer scaffolds. J Bioact Compat Pol **25,** 207, 2010.
15. Xing, Z., Xue, Y., Danmark, S., Schander, K., Ostvold, S., Arvidson, K., Hellem, S., Finne-Wistrand, A., Albertsson, A.C., and Mustafa, K. Effect of endothelial cells on bone regeneration using poly(L-lactide-co-1,5-dioxepan-2-one) scaffolds. J Biomed Mater Res A **96,** 349, 2011.
16. Shimizu, K., Ito, A., and Honda, H. Enhanced cell-seeding into 3D porous scaffolds by use of magnetite nanoparticles. J Biomed Mater Res B Appl Biomater **77,** 265, 2006.
17. Pfaffl, M.W. A new mathematical model for relative quantification in real-time RT-PCR. Nucleic Acids Res **29,** e45, 2001.
18. Chomczynski, P. Shelf-stable product and process for isolating RNA, DNA and proteins. USA: Google Patents; 1993.
19. Mountziaris, P.M., and Mikos, A.G. Modulation of the inflammatory response for enhanced bone tissue regeneration. Tissue Eng Part B Rev **14,** 179, 2008.
20. Costa, C., Incio, J., and Soares, R. Angiogenesis and chronic inflammation: cause or consequence? Angiogenesis **10,** 149, 2007.
21. Shultz, L.D., Schweitzer, P.A., Christianson, S.W., Gott, B., Schweitzer, I.B., Tennent, B., McKenna, S., Mobraaten, L., Rajan, T.V., Greiner, D.L., and Leiter, E.H. Multiple defects in innate and adaptive immunologic function in NOD/LtSz-scid mice. J Immunol **154,** 180, 1995.
22. Waterman, R.S., Tomchuck, S.L., Henkle, S.L., and Betancourt, A.M. A new mesenchymal stem cell (MSC) paradigm: polarization into a pro-inflammatory MSC1 or an Immunosuppressive MSC2 phenotype. PLoS One **5,** e10088, 2010.
23. Romieu-Mourez, R., Francois, M., Boivin, M.N., Bouchentouf, M., Spaner, D.E., and Galipeau, J. Cytokine modulation of TLR expression and activation in mesenchymal stromal cells leads to a proinflammatory phenotype. J Immunol **182,** 7963, 2009.
24. Pevsner-Fischer, M., Morad, V., Cohen-Sfady, M., Rousso-Noori, L., Zanin-Zhorov, A., Cohen, S., Cohen, I.R., and Zipori, D. Toll-like receptors and their ligands control mesenchymal stem cell functions. Blood **109,** 1422, 2007.
25. Hijiya, N., Miyake, K., Akashi, S., Matsuura, K., Higuchi, Y., and Yamamoto, S. Possible involvement of toll-like receptor 4 in endothelial cell activation of larger vessels in response to lipopolysaccharide. Pathobiology **70,** 18, 2002.
26. Mantovani, A., Sica, A., Sozzani, S., Allavena, P., Vecchi, A., and Locati, M. The chemokine system in diverse forms of macrophage activation and polarization. Trends Immunol **25,** 677, 2004.
27. Trindade, R., Albrektsson, T., Tengvall, P., and Wennerberg, A. Foreign body reaction to biomaterials: on mechanisms for buildup and breakdown of osseointegration. Clin Implant Dent Relat Res doi: 10.1111/cid.122274, 2014.
28. Sung, H.J., Meredith, C., Johnson, C., and Galis, Z.S. The effect of scaffold degradation rate on three-dimensional cell growth and angiogenesis. Biomaterials **25,** 5735, 2004.
29. Bartaula-Brevik, S., Pedersen, T.O., Blois, A.L., Papadakou, P., Finne-Wistrand, A., Xue, Y., Bolstad, A.I., and Mustafa, K. Leukocyte transmigration into tissue-engineered constructs is influenced by endothelial cells through toll-like receptor signaling. Stem Cell Res Ther **5,** 143, 2014.

30. Tazzyman, S., Lewis, C.E., and Murdoch, C. Neutrophils: key mediators of tumour angiogenesis. Int J Exp Pathol **90,** 222, 2009.
31. Matsui, A., Yokoo, H., Negishi, Y., Endo-Takahashi, Y., Chun, N.A., Kadouchi, I., Suzuki, R., Maruyama, K., Aramaki, Y., Semba, K., Kobayashi, E., Takahashi, M., and Murakami, T. CXCL17 expression by tumor cells recruits CD11b+Gr1 high F4/80- cells and promotes tumor progression. PLoS One **7,** e44080, 2012.
32. Hirota, K., and Semenza, G.L. Regulation of angiogenesis by hypoxia-inducible factor 1. Crit Rev Oncol Hematol **59,** 15, 2006.
33. Eltzschig, H.K., and Carmeliet, P. Hypoxia and inflammation. N Engl J Med **364,** 656, 2011.
34. Huang, L.E., Gu, J., Schau, M., and Bunn, H.F. Regulation of hypoxia-inducible factor 1alpha is mediated by an O_2-dependent degradation domain via the ubiquitin-proteasome pathway. Proc Natl Acad Sci U S A **95,** 7987, 1998.
35. Huang, L.E., Arany, Z., Livingston, D.M., and Bunn, H.F. Activation of hypoxia-inducible transcription factor depends primarily upon redox-sensitive stabilization of its alpha subunit. J Biol Chem **271,** 32253, 1996.
36. Brune, B., and Zhou, J. The role of nitric oxide (NO) in stability regulation of hypoxia inducible factor-1alpha (HIF-1alpha). Curr Med Chem **10,** 845, 2003.
37. Melillo, G., Musso, T., Sica, A., Taylor, L.S., Cox, G.W., and Varesio, L. A hypoxia-responsive element mediates a novel pathway of activation of the inducible nitric oxide synthase promoter. J Exp Med **182,** 1683, 1995.
38. Karar, J., and Maity, A. PI3K/AKT/mTOR pathway in angiogenesis. Front Mol Neurosci **4,** 51, 2011.
39. Dai, J., Peng, L., Fan, K., Wang, H., Wei, R., Ji, G., Cai, J., Lu, B., Li, B., Zhang, D., Kang, Y., Tan, M., Qian, W., and Guo, Y. Osteopontin induces angiogenesis through activation of PI3K/AKT and ERK1/2 in endothelial cells. Oncogene **28,** 3412, 2009.
40. Lin, C.G., Leu, S.J., Chen, N., Tebeau, C.M., Lin, S.X., Yeung, C.Y., and Lau, L.F. CCN3 (NOV) is a novel angiogenic regulator of the CCN protein family. J Biol Chem **278,** 24200, 2003.
41. Granata, R., Trovato, L., Lupia, E., Sala, G., Settanni, F., Camussi, G., Ghidoni, R., and Ghigo, E. Insulin-like growth factor binding protein-3 induces angiogenesis through IGF-I- and SphK1-dependent mechanisms. J Thromb Haemost **5,** 835, 2007.
42. Dawson, D.W., Volpert, O.V., Gillis, P., Crawford, S.E., Xu, H., Benedict, W., and Bouck, N.P. Pigment epithelium-derived factor: a potent inhibitor of angiogenesis. Science **285,** 245, 1999.

Address correspondence to:
Kamal Mustafa, DDS, PhD
Department of Clinical Dentistry
University of Bergen
Årstadveien 19
5009 Bergen
Norway

E-mail: kamal.mustafa@iko.uib.no

Sushma Bartaula-Brevik, BDS
Department of Clinical Dentistry
University of Bergen
Årstadveien 19
5009 Bergen
Norway

E-mail: sushma.bartaula@iko.uib.no

Received: July 20, 2015
Accepted: November 17, 2015
Online Publication Date: January 14, 2016